
Multiple electrokinetic actuators for feedback control of colloidal crystal size

Jaime J. Juárez,^a Pramod P. Mathai,^{b, c} J. Alexander Liddle^{c*} and Michael A. Bevan^{a*}

5

We report a feedback control method to precisely target the number of colloidal particles in quasi-2D ensembles and their subsequent assembly into crystals in a quadrupole electrode. Our approach relies on tracking the number of particles within a quadrupole electrode, which is used in a real-time feedback control algorithm to dynamically actuate competing electrokinetic transport mechanisms. Particles are removed from the quadrupole using DC-field mediated electrophoretic-electroosmotic transport, while high-frequency AC-field mediated dielectrophoretic transport is used to concentrate and assemble colloidal crystals. Our results show successful control of the size of crystals containing 20 to 250 colloidal particles with less than 10% error. Assembled crystals are characterized by their radius of gyration, crystallinity, and number of edge particles to demonstrate the expected size dependent properties. Our findings demonstrate successful ensemble feedback control of the assembly of different sized colloidal crystals using multiple actuators, which has broad implications for control over nano- and micro- scale assembly processes involving colloidal components.

^aChemical and Biomolecular Engineering, Johns Hopkins University, Baltimore, MD 21218, ^bMaryland Nanocenter, University of Maryland, College Park, MD 20742, ^cNational Institute for Standards and Technology, Center for Nanoscale Science and Technology, 100 Bureau Drive, Gaithersburg, MD 20899
E-mail: mabevan@jhu.edu, liddle@nist.gov

Introduction

The ability to program, reconfigure, control, and manipulate microscopic particles within materials and devices is critical to enable numerous emerging nano- and micro- technologies. As a result, there is considerable effort devoted to programming the interactions between colloids so that when components are mixed together they spontaneously self-assemble.¹ As a complementary approach to *self*-assembly, external fields can be used to manipulate colloids in directed-assembly processes. For example, magnetic fields can be used to manipulate the assembly of particles with permanent or induced magnetic dipoles.² DC and AC electric fields can be used to manipulate colloidal particles using a variety of transport mechanisms. Dielectrophoresis is one such mechanism that can manipulate particles in a diverse range of nano- and bio- applications,^{3,4} including atypical devices such as reconfigurable antennas.⁵ Other electric field mediated mechanisms, including electrophoresis,⁶ electroosmosis,⁷ diffusiohoresis⁸, dipolar chaining,⁹ and dipole transport³ are also available, but have only been used in isolation, limiting the degree of control that can be achieved. Despite the opportunity to implement several actuation mechanisms within a single device, to the authors' knowledge, manipulation of colloidal particles to date has involved only the use of single mechanisms.

Precise control has been demonstrated in the past by manipulating individual particles.¹⁰ For example, optical forces can be used to manipulate individual particles, or many individual particles for colloidal crystal assembly¹¹ and to make functioning microfluidic pumps.¹² Holographic optical tweezers¹³ can be used to simultaneously manipulate several particles at once at laser intensity maxima,¹⁴ but each particle must be individually addressed. Scanning probe methods have been used to manipulate single atoms¹⁵ and molecules,¹⁶ but have seen limited applications to ensembles, other than altering polymer crystallization.¹⁷ Electrode arrays have been used to generate electroosmotic flow patterns with sufficient degrees of freedom to allow control over several non-interacting particle trajectories,¹⁸ where each particle is addressed by independent flow modes. While the techniques described above have proven their utility in numerous applications, scaling them to deal with large numbers of particles is not only extremely challenging, but is not even desirable when there is no requirement for single-particle specificity.

In many instances it is also necessary to control the number of colloidal components involved in assembly processes to create finite-sized objects. Control over the number of particles enables the creation of reproducible cluster microstructures and morphologies, which can affect cluster properties and behavior in subsequent applications and device integration.¹⁹ There are also fundamental questions regarding finite sized structures in terms of the thermodynamics²⁰ and kinetics²¹ that control their assembly. The majority of approaches to date for controlling size of assembled structures are based on templating, where physical confinement within lithographically patterned surface features^{19,22}

or droplets²³ determines the number of particles in a final cluster configuration. Such approaches are not dynamically tunable and cannot be employed in feedback control schemes or be used as reconfiguration mechanisms within devices. There thus exists a need for methods that can dynamically manipulate collections of particles to enable high-throughput nanostructure fabrication or device reconfiguration.

In this work, we use a planar quadrupole electrode device that switches between electrophoretic/electroosmotic (EPEO) and negative dielectrophoretic (NDEP) actuation to assemble colloidal crystals composed of precise numbers of micron sized colloids (see Fig. 1a). This adapts our recent work on feedback control over colloidal crystallization kinetics using only dielectrophoresis⁴ by constructively integrating an additional EPEO transport mechanism to enable control over colloidal crystal size (although crystallization kinetics are not controlled in this work). Image analysis detects the number of colloids within the quadrupole. This number is used in a feedback loop to dynamically control either EPEO (via a DC field) to remove particles or NDEP (via an AC field) to transport particles towards the quadrupole center. After using feedback control over these opposing actuators to obtain a target number of particles, NDEP is used to compress colloids into 2D crystals in the quadrupole center. The final crystals are characterized in terms of their size dependent radius of gyration and crystallinity (that depends on the number of edge and vertex particles). Our results demonstrate a successful approach to manipulate the numbers of particles within ensembles using multiple electrokinetic actuators, which allow for subsequent assembly of well-defined 2D colloidal crystals.

Materials and methods²⁴

Electrode and particle preparation

Coplanar Au thin-film quadrupole electrodes were patterned on microscope coverslips that were washed with isopropanol, KOH, and de-ionized water. The electrodes were fabricated using photolithography with a chrome photomask of the electrode pattern. The thin film consisted of a 15 nm chrome adhesion layer and a 35 nm gold layer deposited with an electron beam evaporator. Photoresist liftoff was done using a remover heated to 80°C with gentle agitation. The quadrupole electrode device was connected in series with a function generator to generate AC electric fields and DC offsets. The device was interfaced using wires attached to the electrode pads with conductive tape. A 2 μL concentrated dispersion of nominal 3.13 μm diameter SiO₂ colloids functionalized with hydroxyl groups was diluted in a mixture of de-ionized water (450 μL) and methanol (50 μL). The average particle concentration was sufficiently high so that the initial number of particles in the quadrupole was always higher than that needed for the targeted crystal sizes. A polydimethylsiloxane O-ring was placed on top of the electrode device to hold 100 μL of the dilute dispersion. The cell was sealed with a cover slip and the dispersion was allowed to sediment for 15 minutes.

Microscopy Experiments

Optical microscopy experiments were performed using an inverted microscope and a 40 \times objective. Videos were captured at

30 frames per second (640 pixels \times 480 pixels, 118 μm \times 89 μm) with an 8-bit charge coupled device (CCD) camera using image acquisition software. Particle centers were tracked in real-time using standard algorithms.²⁵ Computation of order parameters from particle coordinates for the number of crystalline bonds to neighboring particles averaged over all particles, $\langle C_6 \rangle$, and the radius of gyration, R_g , is described in detail in our previous papers.²⁶ The number of edge particles, NE, in a given crystalline configuration is estimated as the number of particles with $C_6 < 6$ (see Supplemental Information for details). Real-time control of the function generator was performed using a software interface. A sinusoidal voltage with a 1 MHz frequency actuated NDEP, and DC offsets were used to actuate EPEO.

Results and discussion

Quadrupolar EPEO and NDEP actuators

Fig. 1a depicts the thin Au film quadrupole electrode patterned onto a microscope slide, which allows for real-time observation in an optical microscope and control over AC electric field amplitudes and frequencies via a function generator. The ability to quantitatively track particle centers and control the electric field in real-time using software enables feedback control over the number of particles and colloidal crystals size. Fig. 1b shows 3.13 μm diameter SiO₂ colloids within the quadrupole center in an AC electric field potential at 1 MHz, 4 V, which can be used to reversibly compress particles into quasi-2D crystalline configuration as we have demonstrated in our previous studies.^{4, 26-30}

The number of particles within the quadrupole center is controlled using two different electric field-mediated interactions. When DC biases are applied to the electrodes, electrophoresis and electroosmosis (EPEO) occur simultaneously to transport particles out of the quadrupole center. Electrophoresis (EP) transports negatively charged SiO₂ particles away from anodes towards cathodes in DC and low frequency fields. Electroosmosis (EO) moves particles in the opposite direction to oppose EP,³¹ which leads to a net transport process that is the superposition of both contributions (see Supplemental Information). The net result is the low Reynolds number transport of particles in a saddle-shaped extensional flow with a stagnation point at the quadrupole center. This transports particles out of the quadrupole center over the electrode edges, which is used to reduce their number within the quadrupole. Fig. 1c shows the quantitative connections based on theoretical expressions in Supplemental Information with a vector plot of the local EPEO transport and a contour plot of the local electric potential.³²

Negative dielectrophoresis (NDEP) is used to concentrate particles in the quadrupole as an actuator that operates in opposition to EPEO. NDEP is actuated by applying an AC electric field at 1 MHz where the horizontal electrodes have the same polarity and the vertical electrodes have the opposite polarity within a single AC cycle. The AC electric field induces dipoles on the silica colloids, which results in their transport to the electric field minimum located in the quadrupole center.^{4, 26-30} As captured by theoretical expressions for NDEP^{26, 27, 29, 30} given in the Supplemental Information, the non-dimensional dipole energy³³ depends on the magnitude of the electric field. In

addition, a term referred to as the Clausius-Mosotti factor (f_{cm}) provides a non-dimensional comparison of particle and media frequency dependent dielectric spectra.³⁴ The sign of f_{cm} at a

given frequency indicates whether particles are more ($f_{cm} > 0$) or less ($f_{cm} < 0$) polarizable than the medium and transported to field

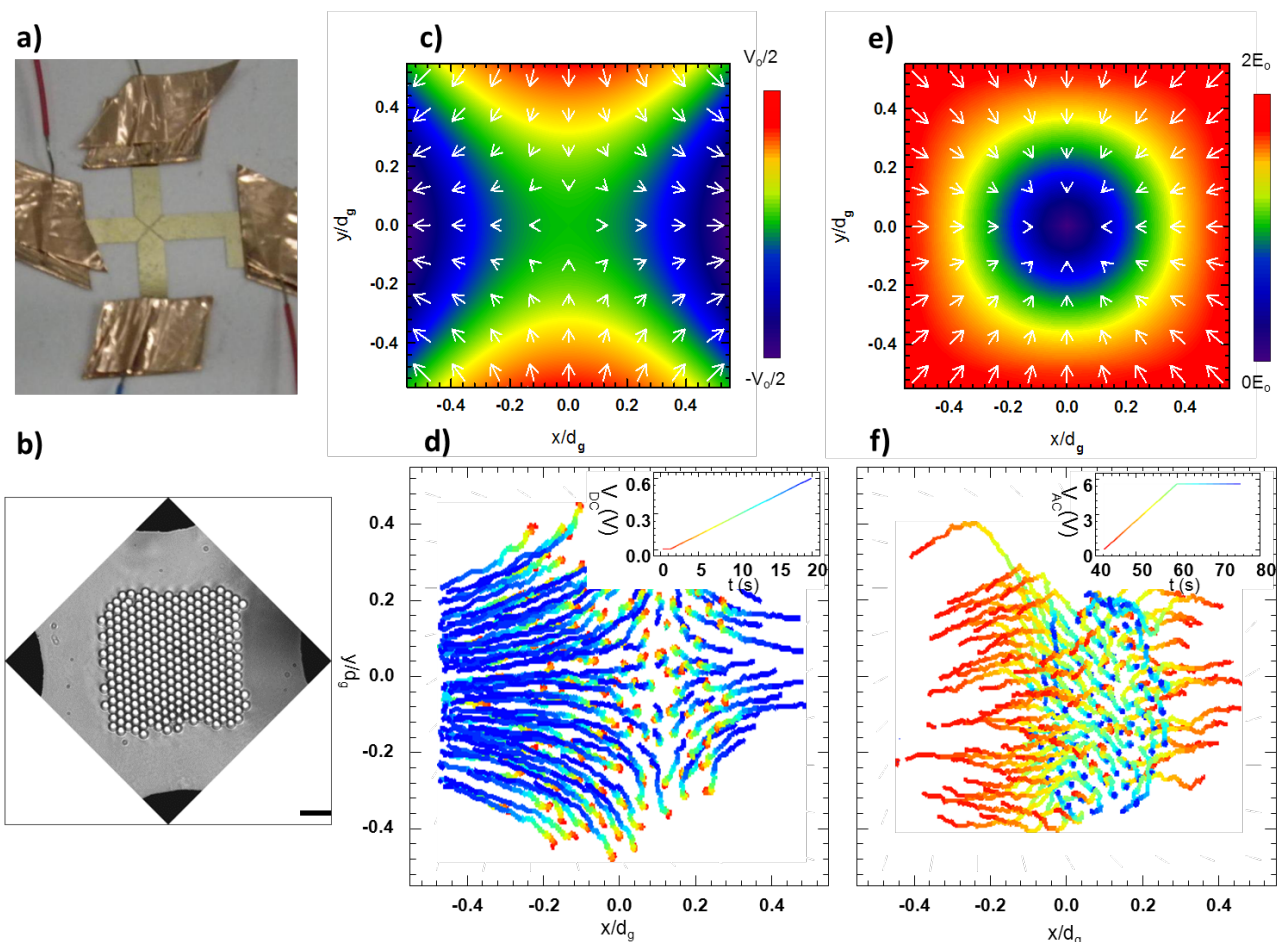


Fig. 1 Electrokinetic control of colloidal ensembles in an interfacial quadrupole electrode. (a) Au thin film quadrupolar electrode on a glass microscope slide. In experiments, a PDMS O-ring containing an aqueous dispersion of colloidal particles is placed above the central control region. Particle centers are tracked in real-time and controlled using a function generator in a feedback loop. (b) Optical microscopy-CCD image of quasi-2D crystal of 3 μm silica colloids in quadrupole with an applied AC electric field potential at 1 MHz, 4 V. Scale bar is 20 μm . (c) Vector plot of electrophoretic-electroosmotic (EPEO) trajectories superimposed on contour plot of the electric field potential. Here, V_0 is the applied potential, d_g is the characteristic spacing between quadrupole electrodes, and $E_0 = V_0/d_g$. (e) Vector plot of negative dielectrophoretic (NDEP) trajectories superimposed on contour plot of the electric field magnitude. The 8-bit linear color scale in (c) and (d) shows the normalized non-dimensional electric field potential and magnitude. Measured particle trajectories for (d) EPEO and (f) NDEP actuation (scale, 56 μm x 54 μm) with trajectories color coded to match temporal voltage profiles inset into each plot.

maxima ($f_{cm} > 0$, positive dielectrophoresis) or minima ($f_{cm} < 0$, NDEP). At 1 MHz, the 3.13 μm SiO_2 colloids experience NDEP and are transported to the electric field minimum at the quadrupole center where they hexagonally close pack into 2D colloidal crystals under compression.^{4, 26-28, 30} Fig. 1c shows the quantitative connections based on the theoretical expressions in the Supplemental Information with a vector plot of the local NDEP force at 4 V and a contour plot of the local electric field magnitude. It should be noted that dipole-dipole interactions have no net contribution to the crystallization process as discussed in detail in our previous papers.^{26,27,29,30}

Trajectories in Figs. 1d and 1f illustrate the dynamic characteristics of ensemble particle transport using the EPEO and NDEP actuators in this case of a 100 particle target. The spatial particle and voltage trajectories are both reported using a linear

spectrum color scale depicting time (see figure caption for details). In Fig. 1d, ramping V_{DC} with no V_{AC} causes particle trajectories to closely mimic the predicted extensional, saddle-shaped flow predicted in Fig. 1c. The simultaneous temporal and voltage information in Fig. 1d also show: (1) when $V_{DC} < 300$ mV they fail to generate sufficient EPEO to transport particles (red-yellow trajectory), (2) when V_{DC} are ramped to > 300 mV the resultant EPEO rapidly transports particles out of the quadrupole at an increasing rate with increasing voltage (green-violet trajectory). In Fig. 1f, the particle trajectories originating from the horizontal electrode edges move into the potential well via NDEP (Fig. 1e) where they remain compressed into a static crystal configuration with application of a constant voltage. The V_{AC} amplitude dependence of the trajectories in Fig. 1f also show: (1) as soon as V_{AC} is initiated particles rapidly converge (<

10 s) under the influence of strong NDEP force (red-yellow trajectory), (2) crystallization occurs on a very short time-scale (green-blue trajectory), and (3) the crystal remains localized with

finite thermal motion on lattice positions in the presence of the static elevated voltage.

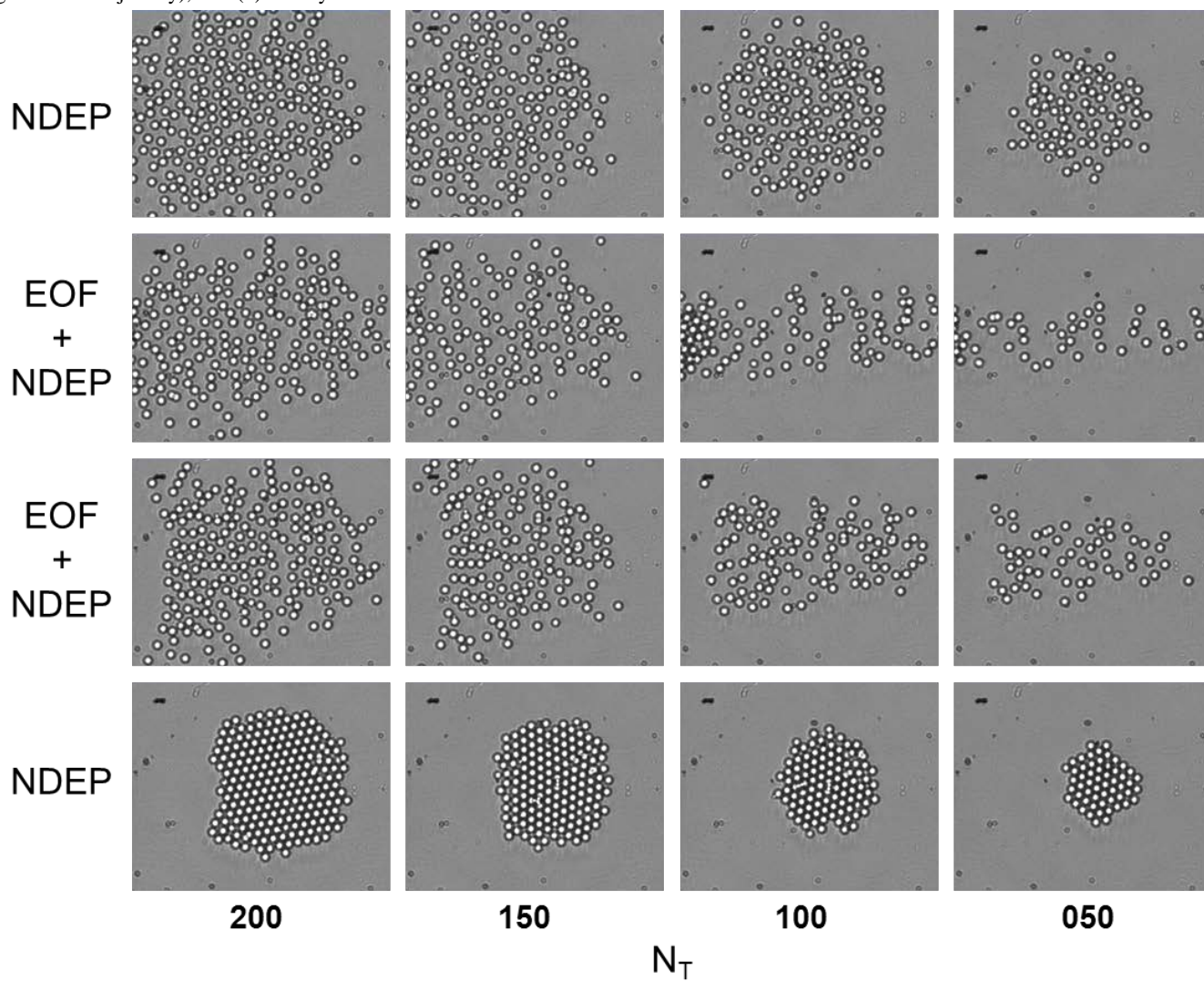


Fig. 2 Matrix of images for four target crystal sizes. In each case, (top row) the initial configuration is a fluid weakly held by NDEP, (2nd & 3rd rows) EPEO and NDEP are cycled via feedback control to iteratively remove and concentrate particles, (bottom row) NDEP is increased to compress particles into quasi-2D colloidal crystals. The inset scale bar is 20 μm .

Quantitative feedback control of particle number

We now show how the EPEO and NDEP actuators described in Fig. 1 can be used to control the number of particles in the quadrupole and their subsequent assembly into 2D crystals. Fig. 2 shows a matrix of static snapshots from movies of a single experiment where the number of 3.13 μm SiO_2 particles within the quadrupole is changed from 200 to 50 in steps of 50 and a crystal is assembled at each step. Movies of the individual step changes are included with Supplemental Information at a rate 10 \times faster than real time. Before describing the quantitative algorithm used to control the number of particles in the quadrupole, we first conceptually describe how the actuators are used together in a stable fashion.

We begin each control cycle with an excess number of

particles weakly held within the quadrupole as a fluid configuration using NDEP (top row of Fig. 2). After selecting a target number of particles smaller than the number within the quadrupole, EPEO is actuated by ramping V_{DC} to transport particles out of the quadrupole as depicted in Figs. 1C and E. When the targeted number of particles is approached within a preset tolerance, NDEP is actuated by ramping V_{AC} (at 1 MHz) to pull the remaining particles within the quadrupole back toward the center as depicted in Figs. 1D and F. Particles that we remove from the quadrupole by EPEO do not re-enter the quadrupole when NDEP is actuated. This scheme can be actuated several times to attain the targeted particle number (middle two rows). After the target number of particles is reached, NDEP is ramped to a maximum and held there to produce a quasi-2D colloidal crystal containing the target number of particles (bottom row).

Several additional empirical observations influence the

quantitative control algorithm that was implemented. When a large number of particles (> 50) were transported away from the quadrupole center using EPEO, some aggregation was observed near the electrode edges. This interfered with subsequent steps to remove more particles. Although the mechanism of this aggregation process was not explored in detail, electrophoretic deposition is expected to control particle aggregation above the electrode surfaces.³⁵ To avoid this issue, particles were removed from the quadrupole region in batches of < 50 particles at a time. Compression of particles into a crystal was not actuated until the target particle number was reached.

The step changes are given by an empirical quantitative control algorithm designed to act on V_{AC} and V_{DC} as a function of time and particle number. The EPEO removal is actuated using,

$$V_{DC}(t) = (t - t_0)C_1, N > 1.1N_T \quad (1)$$

$$V_{AC}(t) = C_2, N > 1.1N_T$$

where t is the elapsed time in seconds after control is initiated at t_0 to achieve a target number of particles N_T , $C_1 = 0.15$ V/s is the rate at which voltage is changed, $C_2 = 0.05$ V is a constant, and N is the instantaneous number of particles. The rate of increase in V_{DC} reflects a 5 mV increase every 33 ms (i.e. the CCD camera frame rate). The value of V_{DC} was not allowed to exceed 0.8 V. When the instantaneous number of particles reaches the target number, NDEP is actuated using,

$$V_{DC}(t) = 0.4(t_1 - t_0)C_1 + (t_1 - t)C_1, N \leq 1.1N_T \quad (2)$$

$$V_{AC}(t) = 2C_2 + 10(t - t_1)C_1, N \leq 1.1N_T$$

where t_1 is time after N becomes less than N_T . The maximum value of V_{AC} was fixed at $(6 - N_T/70)$ V, and the minimum value of V_{DC} was set at 0 V.

The parameters in Eqs. (1) and (2) were obtained empirically. Rates of change and the maximum V_{DC} values were found to maintain control stability with minimal overshoot. The maximum value of V_{AC} was determined as a value sufficient to compress particles into quasi-2D crystalline configurations²⁷ without buckling into the third dimension normal to the substrate.²⁶ A positive 10% bias in the target number of particles (i.e. $1.1N_T$) was necessary because we did not control the rate at which particles exit the quadrupole (i.e. C_1 is a constant) and no electrokinetic mechanism was available to return particles from outside the electrodes back into the quadrupole. EP of particles outside the quadrupole above the electrodes only produces motion normal to the surface and lateral clustering,³⁵ and NDEP only concentrates particles already contained within the electrode boundaries.

Results in Fig. 3 demonstrate how the control algorithm works in practice over a broad range of ensemble sizes. Starting from an ensemble of 267 particles, the results in Fig. 3A show time traces for N , N_T , V_{AC} , and V_{DC} for a series of $N_T = 200, 150, 100, 75, 50,$ and 20 obtained from a single experiment. Results in Fig. 3B show an expanded view of the same traces in Fig. 3A for $N_T = 100$. In between assembling each targeted crystal size in Fig. 3, assembled crystals from the previous step are given 60 s to melt into a fluid configuration in a field with a potential of $V_{AC} = 50$ mV that only weakly holds the particles within the quadrupole via

NDEP (as shown in the top column of Fig. 2).

It is apparent in the V_{DC} and V_{AC} traces is that the two voltages are used to actuate EPEO and NDEP between 1 to 4 times during each portion of the control cycle for $N > N_T$. The reason for this is that, once V_{DC} reaches zero, a transient allows particles that were already removed from the quadrupole, but that remained near the electrode edge, to move back into the quadrupole. The exact origin of this effect was not identified, although a small NDEP contribution or backflow are potential sources (inertial effects can be ruled out due to the low Reynolds number flow in this work). The algorithm in Eqns. (1) and (2) actuates between EPEO and NDEP several times to remove the excess particles that flowed back in. Fig. 3B shows how the alternation between EPEO and NDEP is automated to achieve the condition $N < 1.1N_T$.

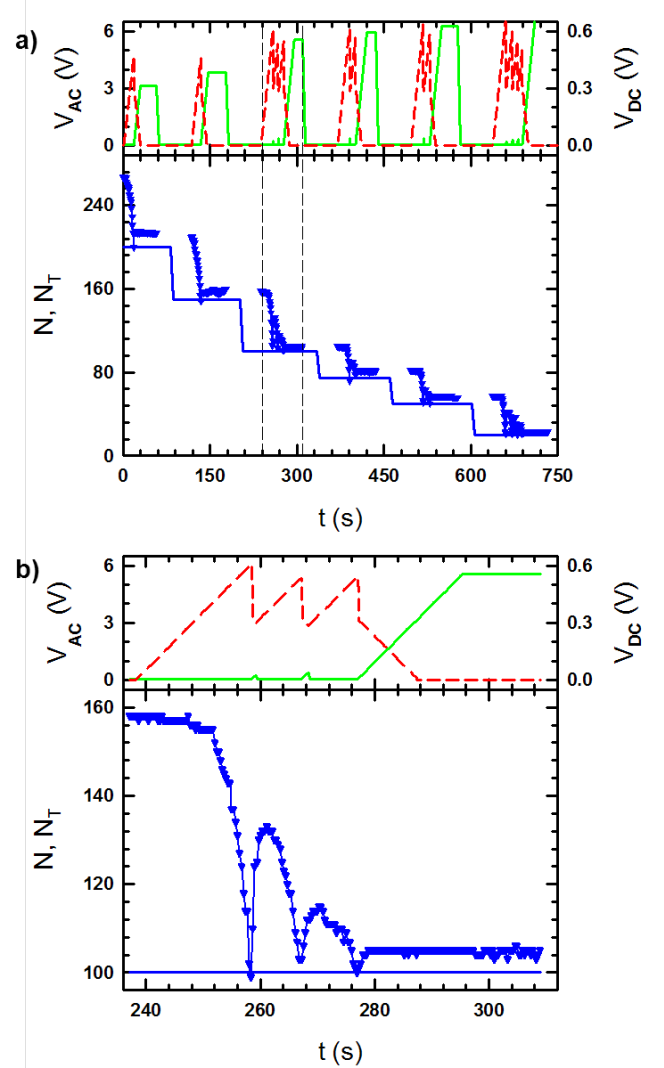


Fig. 3 (a) Series of experiments (blue triangles) showing control algorithm for different target crystal sizes (blue solid line). The two electrokinetic actuators are represented by the voltage cycles between V_{DC} (red dashed line) and V_{AC} (green solid line). (b) Zoom of region between black dashed lines in Fig 3a for the 100 particle target (using same color scheme as 3a).

Controlling crystal size and morphology

Figs. 1-3 show how opposing electrokinetic actuators and an empirical control algorithm can be used to control the number of

particles in a quadrupole. Since we have previously demonstrated that the quadrupole configuration can also be used to control colloidal crystallization using NDEP alone,^{4,26,28} it is now possible to assess the effectiveness of using EP/EO and NDEP together to control the number of particles within assembled crystals. In addition, because the number of particles in a crystal and its overall morphology determine its physical size and degree of hexagonal packing (due to edge effects), we also assess size dependent properties of the assembled crystals using several different metrics. In the following, we report results characterizing the ability to obtain different target crystal sizes and compare their size and morphology dependent crystal properties to theoretical predictions.

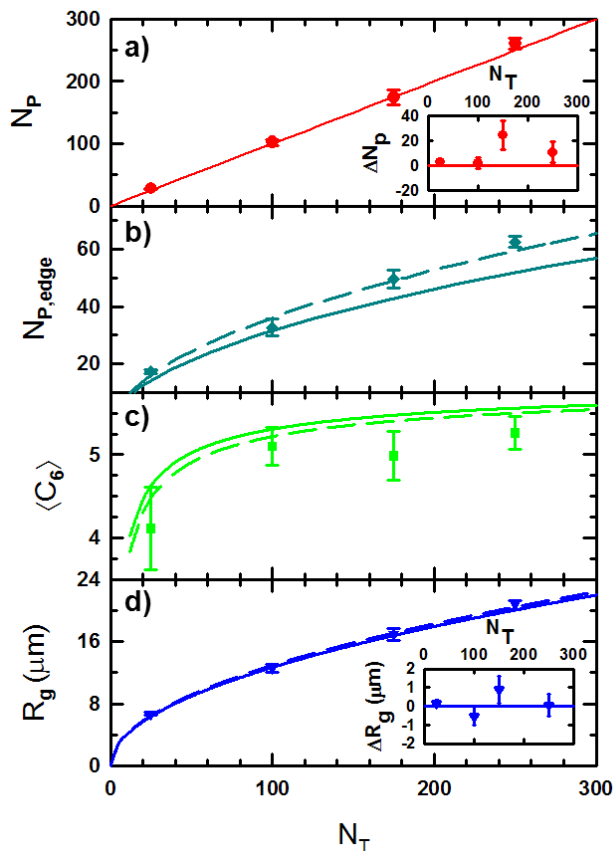


Fig. 4 (a) Average number of particles for four different target crystal sizes (red circles) and the standard deviation (error bars) for five experiments vs. target size (red solid line). Inset shows the difference between experiment and the target size. (b) The number of crystals edge particles for four different target crystal sizes (cyan diamonds) vs. predictions for hexagonal (solid cyan line) and square (dashed cyan line) morphologies. (c) Size dependent average hexagonal order, $\langle C_6 \rangle$, (green squares) vs. predictions for hexagonal (solid green line) and square (dashed green line) morphologies. (d) Radius of gyration (blue triangles) vs. predictions for crystals with hexagonal (solid blue line) and square (dashed blue line) morphologies. Inset shows the difference between measured and predicted R_g for the hexagonal morphology.

Fig. 4 reports, as a function of N_T , data for the actual number of particles obtained in experiments and three order parameters, N_E , R_g and $\langle C_6 \rangle$, that characterize the resulting crystal size and morphology. Fig. 4a demonstrates the reproducibility of particle assembly obtained by showing mean and standard deviations

obtained from multiple trials for the actual number of particles within assembled crystals. The control is robust in the presence of aggregates of a few particles and a control update time limited by the CCD camera speed and image analysis processing rates. Although the particles within aggregates cannot be separated to control the number of particles in the quadrupole, the particle tracking algorithm still identifies individual particles within an aggregate to get an accurate count of N .

Fig. 4b compares predictions for the number of particles at the crystal edge, N_E , based on hexagonal and square morphologies to experimental observations. The number of particles with $C_6 < 6$ is a reliable estimate of the number of edge particles, N_E , because of the high degree of crystalline order we observe in the interior of the assembled structures. The N_E values in Fig. 4b most strongly distinguish between the hexagonal and square morphologies. In particular, the N_E results are closer to hexagonal morphology predictions for smaller system sizes and closer to the square morphology predictions for larger system sizes. This result is expected, because the electric field has essentially no angular variations in the quadrupole center. A hexagonal morphology can be expected for smaller system sizes localized in the quadrupole center region. In contrast, the increasingly quadrupolar field shape sampled by larger ensembles away from the center region and closer to the electrode edges could be expected to favor a four-fold square morphology.

Figs. 4c and 4d report the average number of hexagonal close packed neighbors, $\langle C_6 \rangle$, and the radius of gyration, N_E , for the final assembled crystals. Calculation of $\langle C_6 \rangle$ and N_E from particle coordinates is described in our previous papers,²⁶ and theoretical predictions of the size dependence of N_E , $\langle C_6 \rangle$, and R_g for hexagonal and square morphologies are derived in the Supporting Information. The values of R_g in Fig. 4d are close to target values, but unlike N_E the calculated and measured R_g values are relatively insensitive to morphology. For example, the R_g values are quite close to the predictions for both the hexagonal and square morphology crystals, but the predictions are also quite close to each other. Only one parameter is required in the R_g prediction to produce the observed agreement; the effective particle radius, a_{eff} , which takes into account the spacing between colloids due to electrostatic interactions. This was measured via image analysis to have $a_{eff} = (1.72 \pm 0.25) \mu\text{m}$, which is larger than the core particle radius of $a = 1.57 \mu\text{m}$. The average interparticle spacing of 150 nm is consistent with expectations of 5 to 10 Debye lengths for the ionic strengths in these experiments.³⁶

In contrast to N_E and R_g , the $\langle C_6 \rangle$ measurements and predictions all differ from each other to a greater extent, which is based on the sensitivity of this parameter to hexagonal order. Because $\langle C_6 \rangle$ measures the number of bonds between hexagonal close packed neighbors, breaking bonds due to defects, doublets, polydisperse particles, or Brownian motion near the crystal periphery can significantly reduce $\langle C_6 \rangle$ compared to the predictions for perfect, athermal crystals. As a result, the $\langle C_6 \rangle$ prediction should be viewed as an upper bound, which our results approach within the limits of the effects already mentioned. Ultimately, even with the sensitivity of $\langle C_6 \rangle$ to experimental non-idealities, the agreement between measurements and predictions in Fig. 4b is quite good. Clearly, the ability to control the number

of particles with multiple electrokinetic actuators provides the capability to assemble quasi-2D crystals with the expected microstructural and morphological properties.

Some hardware and software limitations in our current implementation could be overcome to enable improved control over particle number in future work. For example, the CCD camera frame rate is comparable to the dynamics in these experiments. A higher speed camera would compensate for either increased diffusion rates of smaller nanoparticles or the faster migration rates resulting from stronger fields.³⁷ Tracking particle centers is the most computationally intensive and slowest step (e.g. 16 ms for 250 particles) in the controller algorithm. As a result, faster particle tracking algorithms would be required for faster moving or larger numbers of particles. However, for larger ensembles, it may not be necessary to track each particle. Instead, the ensemble size could be monitored directly, using the intensity of transmitted light through the control region. This approach could also be applied to concentrated nanoparticles where the diffraction limit reduces the ability to identify individual particle centers when they are close to each other.

Conclusions

We have demonstrated a robust feedback control method, using multiple actuators, to precisely control the number of particles within a quadrupole electrode device and to subsequently assemble quasi-2D colloidal crystals of predetermined sizes. Particles are removed from the quadrupole center using electrophoretic/electroosmotic (EPEO) actuation while negative dielectrophoresis (NDEP) actuation is used in an opposing fashion to return particles to the quadrupole center. The automated feedback algorithm was implemented using sensing via real-time particle tracking and actuation via AC and DC electric fields that regulated the relative strengths of the NDEP and EPEO transport mechanisms. Control over the number of particles was shown to be effective and robust without optimization of control parameters or the use of sophisticated hardware. After reaching target particle numbers in the quadrupole device, 2D colloidal crystals were assembled. As the size of the crystals was increased, the morphology changed from hexagonal to square, reflecting the loss of field isotropy close to the electrode edges. The coupled use of actuators is not limited to just the two electrokinetic ones demonstrated here. The addition of further orthogonal actuation mechanisms would enable more sophisticated particle manipulation allowing for future extensions of this approach (e.g., system size-dependent nucleation, three dimensional crystals, anisotropic particles, functionalization of particles).³⁸ Finally, the use of photopolymerizable functionalizations could be used to create permanent ensembles with precisely controlled structures.

Acknowledgements

MAB and JJJ acknowledge financial support provided by the National Science Foundation through a Cyber Enabled Discovery and Innovation grant (CMMI-0835549) and an unsolicited grant (CBET-0932973), the Air Force Office of Scientific Research (FA9550-08-1-0329), and the National Institute of Standards and Technology (70NANB10H198). PPM acknowledges support

under the Cooperative Research Agreement between the University of Maryland and the National Institute of Standards and Technology Center for Nanoscale Science and Technology, Award 70NANB10H193, through the University of Maryland. JJJ and PPM acknowledge helpful discussions with Andrew Berglund and help with the experimental set up from Alan Band, Gerard Henein, Glenn Holland, and Chet Knurek.

References

- † Electronic Supplementary Information (ESI) available: [details of any supplementary information available should be included here]. See DOI: 10.1039/b000000x/
- 1 S. Y. Park, A. K. R. Lytton-Jean, B. Lee, S. Weigand, G. C. Schatz, C. A. Mirkin, *Nature* 2008, 451, 553; A. J. Kim, R. Scarlett, P. L. Biancaneello, T. Sinno, J. C. Crocker, *Nat. Mater.* 2009, 8, 52; H. Gu, J. Chao, S.-J. Xiao, N. C. Seeman, *Nature* 2010, 465, 202.
 - 2 L. E. Helseth, H. Z. Wen, R. W. Hansen, T. H. Johansen, P. Heinig, T. M. Fischer, *Langmuir* 2004, 20, 7323; R. M. Erb, H. S. Son, B. Samanta, V. M. Rotello, B. B. Yellen, *Nature* 2009, 457, 999; A. Snezhko, I. S. Aranson, *Nat. Mater.* 2011, 10, 698.
 - 3 R. Pethig, *Biomicrofluidics* 2010, 4, 022811.
 - 4 J. J. Juarez, M. A. Bevan, *Advanced Functional Materials*, accepted 2012.
 - 5 P. Bahukudumbi, W. N. Everett, A. Beskok, G. H. Huff, D. Lagoudas, Z. Ounaies, M. A. Bevan, *Appl. Phys. Lett.* 2007, 90, 224102.
 - 6 A. E. Cohen, *Phys. Rev. Lett.* 2005, 94; M. Trau, S. Sankaran, D. A. Saville, I. A. Aksay, *Nature* 1995, 374, 437.
 - 7 M. Armani, S. Chaudhary, R. Probst, B. Shapiro, *Journal of Micro-Electro-Mechanical Systems* 2006, 15, 945.
 - 8 B. Abecassis, C. Cottin-Bizonne, C. Ybert, A. Ajdari, L. Bocquet, *Nat. Mater.* 2008, 7, 785.
 - 9 A. P. Gast, C. F. Zukoski, *Adv. Colloid Interface Sci.* 1989, 30, 153.
 - 10 J. Gorman, B. Shapiro, Eds., *Feedback Control of Systems on the Micro- and Nano-Scales: from MEMS to Atoms*, Springer-Verlag, New York, NY 2010.
 - 11 D. L. J. Vossen, M. A. Plaisier, A. v. Blaaderen, *Colloidal crystallization induced by optical gradient forces exerted by optical tweezers*, Vol. 5514, SPIE, 2004.
 - 12 A. Terray, J. Oakey, D. W. M. Marr, *Science* 2002, 296, 1841; T. Sawetzki, S. Rahmouni, C. Bechinger, D. W. M. Marr, *Proceedings of the National Academy of Sciences* 2008.
 - 13 D. G. Grier, *Nature* 2003, 424, 810.
 - 14 R. W. Bowman, G. Gibson, D. Carberry, L. Picco, M. Miles, M. J. Padgett, *J. Opt.* 2011, 13, 044002.
 - 15 D. M. Eigler, E. K. Schweizer, *Nature* 1990, 344, 524.
 - 16 S. K. Kufer, E. M. Puchner, H. Gump, T. Liedl, H. E. Gaub, *Science* 2008, 319, 594.
 - 17 X. Liu, Y. Zhang, D. K. Goswami, J. S. Okasinski, K. Salaita, P. Sun, M. J. Bedzyk, C. A. Mirkin, *Science* 2005, 307, 1763.
 - 18 M. D. Armani, S. V. Chaudhary, R. Probst, B. Shapiro, *Journal of Microelectromechanical Systems* 2006, 15, 945.
 - 19 Y. Cui, M. T. Björk, J. A. Liddle, C. Sönnichsen, B. Bousset, A. P. Alivisatos, *Nano Letters* 2004, 4, 1093.
 - 20 R. S. Berry, *Nature* 1998, 393, 212; T. L. Hill, *Nano Letters* 2001, 1, 273.
 - 21 D. J. Beltran-Villegas, M. A. Bevan, *Soft Matter* 2011, 7, 3280; D. J. Beltran-Villegas, R. M. Sehgal, D. Maroudas, D. M. Ford, M. A. Bevan, *J. Chem. Phys.* 2011, 135, 154506.
 - 22 Y. Yin, Y. Lu, B. Gates, Y. Xia, *Journal of the American Chemical Society* 2001, 123, 8718.
 - 23 V. N. Manoharan, M. T. Elsesser, D. J. Pine, *Science* 2003, 301, 483.
 - 24 All references to commercial products are provided only to document how results were obtained. Their identification does not imply recommendation or endorsement by NIST.
 - 25 J. C. Crocker, D. G. Grier, *J. Colloid. Interface Sci.* 1996, 179, 298.
 - 26 J. J. Juarez, S. E. Feicht, M. A. Bevan, *Soft Matter* 2011.
 - 27 J. J. Juarez, M. A. Bevan, *J. Chem. Phys.* 2009, 131, 134704.

-
- 28 J. J. Juárez, M. A. Bevan, submitted 2012.
- 29 J. J. Juárez, J.-Q. Cui, B. G. Liu, M. A. Bevan, *Langmuir* 2011, 27, 9211.
- 30 J. J. Juárez, B. G. Liu, J.-Q. Cui, M. A. Bevan, *Langmuir* 2011, 27, 9219.
- 5 31 H. J. Keh, J. L. Anderson, *J. Fluid Mech.* 1985, 153, 417.
- 32 G. R. Janik, J. D. Prestage, L. Maleki, *Journal of Applied Physics* 990, 67, 6050.
- 33 P. M. Adriani, A. P. Gast, *Physics of Fluids* 1988, 31, 2757.
- 10 34 T. B. Jones, *Electromechanics of Particles*, Cambridge University Press, Cambridge 1995; H. Morgan, N. G. Green, *AC electrokinetics: colloids and nanoparticles*, Research Studies Press, Philadelphia, PA 2003.
- 35 S. A. Guelcher, M. A. Bevan, Y. Solomentsev, J. L. Anderson, *Langmuir* 2000, 16, 9208.
- 15 36 H.-J. Wu, T. O. Pangburn, R. E. Beckham, M. A. Bevan, *Langmuir* 2005, 21, 9879.
- 37 S. L. Eichmann, S. G. Anekal, M. A. Bevan, *Langmuir* 2008, 24, 714; S. L. Eichmann, M. A. Bevan, *Langmuir* 2010, 26, 14409; S. L. Eichmann, B. Smith, G. Meric, D. H. Fairbrother, M. A. Bevan, *ACS Nano* 2011, 5, 5909.
- 20 38 N. Yasuda, S. Yamamoto, Y. Wada, S. Yanagida, *Journal of Polymer Science Part A: Polymer Chemistry* 2001, 39, 4196.